ChemComm

Transient Methods for Understanding the Properties of Strongly Oxidizing Radicals

Journal:	*ChemComm*
Manuscript ID	CC-FEA-11-2024-006158.R1
Article Type:	Feature Article

Transient Methods for Understanding the Properties of Strongly Oxidizing Radicals

Dmitry E. Polyansky

Chemistry Division, Brookhaven National Laboratory, Upton, NY 11973-5000, USA.

*email: dep@bnl.gov

Abstract

This review discusses the properties of strongly oxidizing radicals in organic and aqueous media and highlights the challenges in obtaining accurate values of their reduction potentials. Transient redox equilibrium methods based on the use of strong photooxidants or initiated by pulse radiolysis are shown to provide versatile approaches for decoupling electron transfer reactions from follow-up reactivity of unstable radical species, resulting in accurate values of reduction potentials of very positive couples, including some solvent radical cations. We also show that correlations of reduction potentials with Hammett $\Sigma\sigma_p^+$ parameters, as well as gas phase ionization potentials, can be used to estimate the redox properties of unknown couples within a homologous series of compounds. The effects of ion pairing and hemicolligation on redox properties of organic and inorganic radicals are also discussed.

Introduction

Redox active radical intermediates play an important role in a wide range of chemical transformations, including biological activity, synthetic chemistry or energy generation and storage processes. Among those, oxidizing radical species are often involved in redox catalysis, e.g., for water oxidation,[1-3] operation of redox flow batteries,[4, 5] nuclear fuel processing,[6] environmental remediation,[7] photoredox catalysis,[8, 9] molecular machines[10] and many other practical applications. However, despite wide utilization of oxidative radical reactivity, some fundamental properties of highly energetic radicals, especially those of high reactivity, remain underexplored. The transient nature of unstable radical intermediates prevents the use of voltammetry techniques commonly utilized for studying redox properties, which rely on unperturbed redox equilibrium between couples in solution and, for example, an electrode. Fortunately, there are alternative transient methods capable of resolving redox reactions and follow-up radical chemical transformations, which provide a more versatile probe into the properties and reactivity of oxidative intermediates. Our group has been utilizing the technique of pulse radiolysis, together with transient photochemical methods, for the generation of powerful oxidation reagents and their use in the study of charge transfer reactions in systems relevant to redox catalysis and electron (proton coupled) transfer relays.[3, 11] This brief overview of

the oxidative chemistry of transient radicals highlights some challenges related to the generation and characterization of radical species, summarizes the redox properties of several classes of organic and inorganic radicals, and presents some trends in their redox properties, together with examples of mechanistic inquiries into catalytic reactions using oxidative radical chemistry.

Reduction potentials of reactive radicals determined electrochemically. The reduction potential of a redox reagent is arguably its most important property, which is not only linked to the thermodynamics of an electron transfer reaction, but also influences its kinetics. For example, Marcus theory of electron transfer[12] points to an exponential dependence of the electron transfer rate coefficient on the driving force (and hence the reduction potentials of a donor and an acceptor), and this dependence is strongest near an equilibrium, with reaction rates doubling about every ten millivolts. Consequently, the precise determination of reduction potentials is critical for an accurate description of electron transfer reactions, especially when theoretical models are based on free energy relationships. Electrochemical methods[13, 14] are widely used for obtaining reduction potentials, but they have their own limitations, including: a) possible interference from chemical reactions following an initial electron transfer; b) necessity for an electrolyte; c) limited electrochemical window of certain solvents. The electrochemical behavior of a heterogeneous redox process (E, equation 1) coupled to a homogeneous chemical reaction (C, equation 2) has been thoroughly investigated by Savéant.[14] Savéant has shown that the shape of a cyclic voltammogram (CV) depends on the interplay of electrode scan rate (ν), the equilibrium constant of a follow-up chemical reaction (K), and the rate of achieving the equilibrium ($k = k_f + k_r$, where k_f and k_r are the forward and reverse rate coefficients, respectively). The graphical form of such dependence – a so-called "kinetic zone diagram" (Figure 1), depicts cyclic voltammogram waves in the logarithmic space determined by the equilibrium constant and a dimensionless parameter, λ as defined in eq. 3. The reversible Nernstian wave (red CVs in Figure 1) can be observed only if the contribution of the follow-up chemical reaction is small (low value of K) or the scan rates are high (large ν), conditions represented by the leftmost and uppermost sections of the zone diagram. The value of $E_{1/2}$ can be obtained from such CVs, which can be closely approximated to the standard reduction potential of a given redox couple. However, if the contribution of a chemical equilibrium is significant, or the scan rate is too low, the resulting quasi-reversible (purple CVs, Fig. 1) or irreversible (blue CV, Fig. 1) waves can provide only approximate values of reduction potentials. Interestingly, when the rate at which equilibrium is established is sufficiently high, a reversible wave is observed even if the contribution of the chemical reaction is significant.

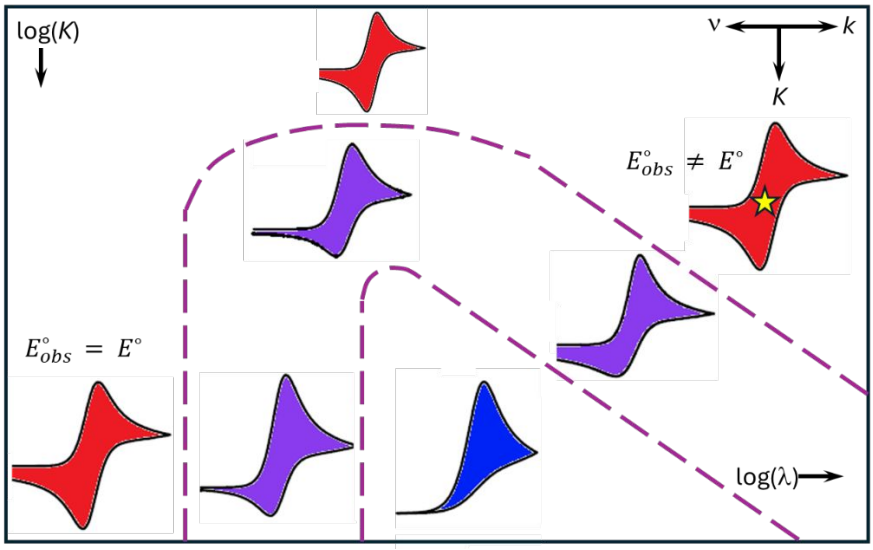

Figure 1. Kinetic zone diagram demonstrating the dependence of the cyclic voltammogram (CV) shape on the electrode scan rate (ν) and the equilibrium constant (K) and rate of establishment of equilibrium ($k = k_f + k_r$) for the following chemical reaction. The red shaded CVs correspond to reversible Nernstian waves; the red shaded CV with a star represents a reversible Nernstian wave with contribution of chemical equilibrium; purple waves are for quasi-reversible and the blue wave is for irreversible electron transfer. The diagram is constructed based on the work by Savéant.[14]

Unfortunately, the observed reduction potential (E°_{obs} in eq. 4, where R is universal gas constant, F is Faraday constant and T is temperature) will contain a contribution of the equilibrium constant for the chemical process and can differ significantly from the standard reduction potential. The last situation can be especially misleading in the determination of reduction potentials if additional care is not taken to examine the diagnostic behavior of peak potential and current in a wide range of scan rates[15, 16] or if other control experiments, e.g., variation of substrate concentration or comparison to the pulsed or AC voltammetry are not performed to insure the absence of a follow-up chemical reactions.

$$\text{E:} \quad A + e^- \overset{k_{ET}}{\rightleftarrows} B \ (E^\circ) \tag{1}$$

$$\text{C:} \quad B \underset{k_r}{\overset{k_f}{\rightleftarrows}} C \ \left(K = \frac{k_f}{k_r}\right) \tag{2}$$

$$\lambda = \frac{RT}{F}\frac{k_f + k_r}{\nu} = \frac{RT}{F}\frac{k}{\nu} \tag{3}$$

$$E^\circ_{obs} = E^\circ + \frac{RT}{F} ln(1 + K) \tag{4}$$

Differential pulse voltammetry or square wave voltammetry are often used for obtaining reduction potentials of quasi-reversible couples when the contribution of the follow-up chemical process is not significant ($K < 10$). However, a more precise criteria for reversibility would vary depending on particular experimental setup configuration (e.g, electrode size) and individual rates of heterogeneous and homogeneous reactions and can be determined from careful analysis of the peak currents and peak potentials as a function of pulse parameters, such as magnitude and duration of applied pulses.[17] In cases where CV waves are fully irreversible, AC voltammetry is more useful for decoupling the scales for electron transfer and interfering chemical reactions. Specifically, Second Harmonic AC Voltammetry (SHACV) has emerged as one of the most powerful electrochemical techniques for analyzing non-Nernstian redox processes.[18-20] It was shown that even in the case of a very fast chemical reaction ($k_f = 10^8$ s^{-1}), the measured E°_{obs} should be within 60 mV of the standard potential, E°.[21] Fukuzumi and Guldi have used SHACV to measure reduction potentials of a series of aromatic cations in the potential range $0.75 - 1.47$ V vs. $Fc^{+/0}$ (ferrocenium/ferrocene reference).[22] They found a good linear correlation between reduction (E°) and ionization potentials (I_p) of aromatic radical cations (Figure 2). However, the slope of this correlation (0.4) was well below unity and the authors have rationalized it by decrease in the solvation energies of the radical cations with lower ionization potentials due to more delocalized nature of an unpaired electron. This proposed effect is not unreasonable since the solvation will affect only reduction potentials in solution, but not gas-phase I_p values. Alternatively, SHACV measurements could underestimate the potentials of most positive couples leading to decrease in the slope of the $E^{\circ} - I_p$ correlation.

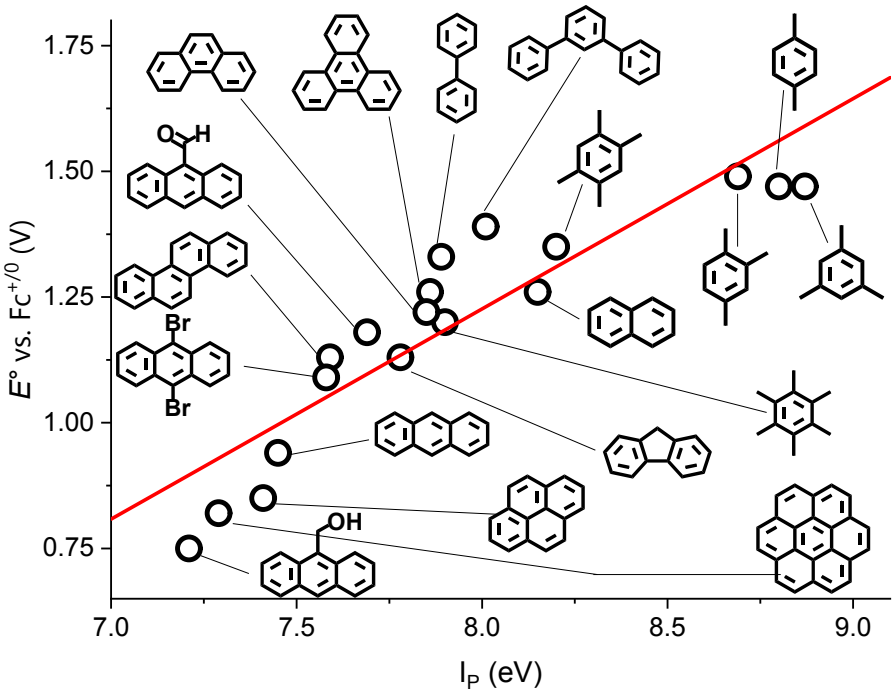

Figure 2. Correlation between reduction potentials of aromatic radical cations mesured using SHACV and their ionization potentials. The red line represents a linear fit. The plot is produced from data reported in ref [22].

Equilibrium methods for determination of reduction potentials. When voltammetry is not suitable for accurate measurements of reduction potentials, they can be determined by measuring an equilibrium constant between a species with unknown potential (U) and a reference compound for which the reduction potential is known (R), as shown in eqs. 5 – 7.

$$U^+ + R \underset{k_r}{\overset{k_f}{\rightleftarrows}} U + R^+ \ (K_{eq}) \tag{5}$$

$$K_{eq} = \frac{[R^+][U]}{[U^+][R]} \tag{6}$$

$$E_U = E_R - 0.059 \log(K_{eq}) \tag{7}$$

This method is applicable even in cases where redox active species are unstable down to sub-microsecond time scales,[23, 24] as long as the rate at which the equilibrium is established ($k_{eq} = k_f[R] + k_r[U]$) exceeds the rate of follow-up chemical reactions and the analytical techniques used for concentration measurements possess sufficient time resolution (Figure 3). This approach is sometimes referred to as

"transient electrochemistry" and allows the decoupling of redox and chemical reactions on timescales not accessible by conventional electrochemical methods.

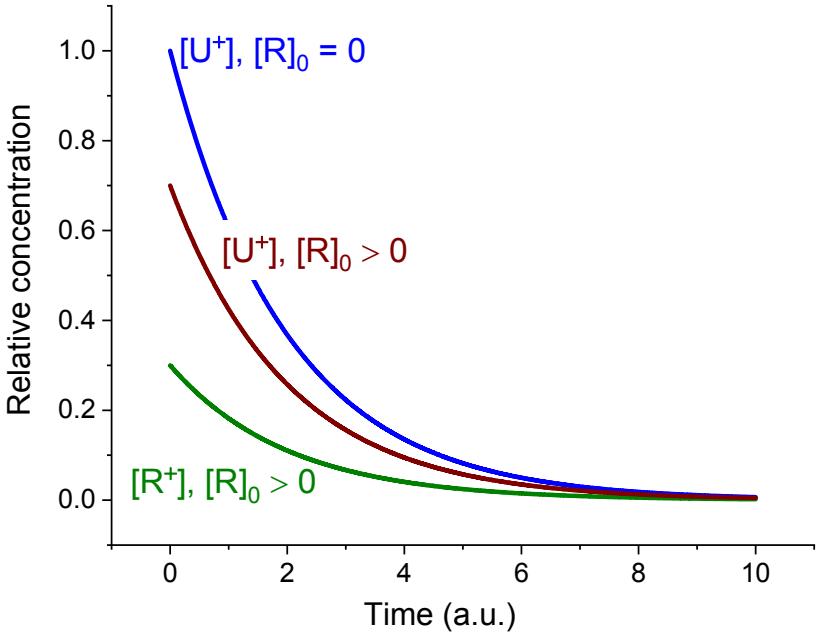

Figure 3. Schematic representation of concentration – time profile of the oxidized form of the species with unknown reduction potential (U^+) in the absence of reference compound R (blue trace). Time dependence of equilibrium concentrations of U^+ (wine) and R^+ (green) under equilibrium conditions. Reprinted with permission from ref [24]. Copyright 2023 American Chemical Society.

Usually, the application of the equilibrium method requires knowledge of equilibrium concentrations of all species in eq. 5. However, if the concentrations of cations are substantially smaller compared to the initial concentration of both species ($[R^+] << [R]_0$; $[U^+] << [U]_0$), equation 6 can be approximated as follows:

$$K_{eq} \approx \frac{[R^+][U]_0}{[U^+][R]_0} \quad (8)$$

This condition is not uncommon during some time-resolved measurements, such as flash photolysis or pulse radiolysis, where only a small amount of starting material is converted to a reduced or oxidized form through initial photoexcitation or ionization events. While specific mechanisms for photochemical or radiolytic generation of redox species are different and their details will be discussed later in this review, both methods rely on the generation of a primary oxidant, such as the oxidative excited state of a chromophore molecule or a solvent radical cation, which is scavenged by R or U, leading to generation of their respective radical cations. Under specific reaction conditions when the total concentration of both

reagents ($[R]_0 + [U]_0$) is constant and sufficiently high to ensure rapid scavenging of the primary oxidant, it can be assumed that the total concentration of radicals produced ($[R^+] + [U^+]$) is the same and independent of the initial concentrations of individual reagents. In this case, an equilibrium constant can be determined from optical absorbance values of the radicals as shown in eq. 9, where Abs(U^+) and Abs(R^+) are optical absorbance values measured during oxidation of U and R only and Abs(UR) is the optical absorbance measured after transient oxidation of a mixture of U and R.[24] This approach does not require the knowledge of extinction coefficients of radical cations and it is applicable even if the absorbances of U^+ and R^+ overlap. However, a small difference in extinction coefficients of radical cations will cause significant errors in *K* due to the small value of the denominator in eq. 9. This simple method is only applicable if the rate coefficients for natural decay of U^+ and R^+ are similar, otherwise a more complex treatment should be used, which is based on analysis of complete decay profiles of individual components and a mixture, and has been described in detail in our recent work.[24]

$$K_{eq} \approx \frac{[U]_0}{[R]_0} \times \frac{Abs\,(U^+) - Abs(UR)}{Abs(UR) - Abs(R^+)} \qquad (9)$$

Another approach for measuring equilibrium constants is based on extracting the rates of forward and reverse reactions between unknown and reference species in eq. 5. Assuming that initial concentrations of R and U are significantly higher compared to the concentrations of radicals, the apparent rate coefficient for change in concentration of R^+ or U^+ can be described by eq. 10. Plotting the apparent rate coefficient as a function of, for example, $[R]_0$, while $[U]_0$ is kept constant should provide a linear dependence with the slope equal to k_f and the intercept equal to $k_r[U]_0$.[25]

$$k_{app} = k_f[R]_0 + k_r[U]_0 \qquad 10$$

However, if radical cations U^+ and R^+ are unstable and decay with rate coefficients k_U and k_R respectively, a more complex kinetic treatment is needed.[26] The solution of the system of differential equations results in the following time dependence of the transient optical absorbance (Δ Abs) of radical cations (eqs. 11-15, where: c_1 and c_2 are pre-exponential terms containing contribution form absorbances of both R^+ and U^+, and c_3 is a fitting parameter to accommodate residual absorbance due to accumulation of permanent products and γ are time constants):

$$\Delta \text{ Abs} = c_1 \exp(-\gamma_1 t) + c_2 \exp(-\gamma_2 t) + c_3 \quad (11)$$

$$\gamma_1 = 0.5(X + Y) + 0.5\sqrt{(X - Y)^2 + 4k_f[R]k_r[U]} \quad (12)$$

$$\gamma_1 = 0.5(X + Y) - 0.5\sqrt{(X - Y)^2 + 4k_f[R]k_r[U]} \quad (13)$$

$$X = k_f[R] + k_U \quad (14)$$

$$Y = k_r[U] + k_R \quad (15)$$

Accurate measurements of large equilibrium constants (e.g., $K_{eq} > 10^3$) can be difficult, as it requires the use of high ratios of initial concentrations or extremely sensitive detection of optical absorbance ratios. In many cases, the difference in reduction potentials of unknown and reference compounds would be limited to ca. 200 mV or less.[24, 27-29] This limitation, however, does not preclude the use of equilibrium methods for obtaining potentials of unknown couples significantly far from known references, but would require the use of a "redox equilibrium ladder" approach, where a series of equilibrium measurements are taken to obtain relative reduction potentials of two compounds separated by a measurable difference in potentials and linking all individual pairs into a single redox ladder (Figure 4). Care should be taken in calculating errors for each individual measurement and propagating these errors along the redox ladder towards high potential couples. The logarithmic dependence of potentials on equilibrium constants helps to attenuate errors in equilibrium measurements.

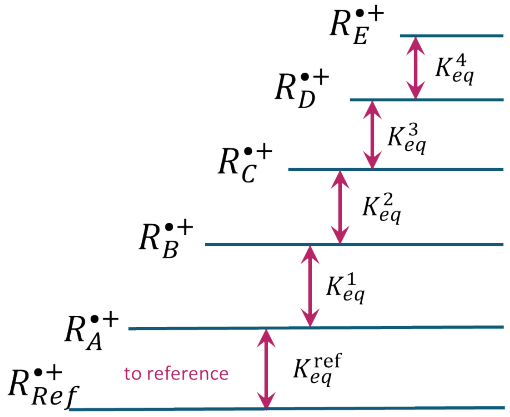

Figure 4. Redox equilibrium ladder for determination of reduction potentials of highly oxidizing radicals.

Photochemical methods for measuring reduction potentials. One of the methods for transient generation of highly oxidizing species involves the use of a photosensitizer, which upon photoexcitation

becomes a strong electron acceptor and can rapidly oxidize added substrates.[8, 9, 30] Simple organic molecules, such as DCA and TCA (Chart 1) have been reported by Goud and Farid[31] as potent photooxidants, with reduction potentials around 2 V vs. SCE ($DCA^{*0/-}$) and 2.4 V vs. SCE ($TCA^{*0/-}$), respectively. These potentials are sufficiently positive for oxidation of a series of substituted benzenes including all three xylene isomers. It was noted however, that the use of neutral sensitizers results in the formation of an ion pair between the reduced sensitizer and oxidized donor molecule D (e.g., $DCA^{\bullet-}\ldots D^{\bullet+}$). This ion pairing complicates the analysis of electron transfer and may require the use of a secondary electron donor, which mediates electron transfer between primary radicals and added substrates. Following this report, the group of Dinnocenzo[23] reported the use of N-methylquinolinium hexafluorophosphate (NMQ^+, Chart 1) as a photooxidant for photochemical generation of aromatic radical cations. Being a charged molecule, NMQ^+ becomes a neutral radical after accepting an electron, which eliminates the complexity of ion pairing with an electron donor, an issue inherent to neutral sensitizers.

Chart 1. Structures of organic photooxidants for production of strongly oxidizing radical cations.

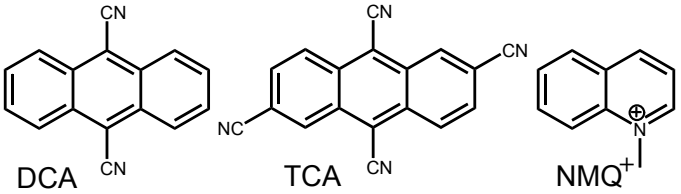

The photochemistry of photooxidants containing iminium cationic functionality ($R_2{-}N^+{=}CR_2$) has been investigated by Mariano and co-workers.[32] They found that quinolinium cations produce strongly oxidizing excited states ($E^{\circ\prime}$ = 2.5 – 2.7 V vs. SCE in CH_3CN) upon UV photoexcitation (λ_{max} = 312 – 336 nm) and pyridinium salts were even stronger photooxidants ($E^{\circ\prime}$ = 3.0 – 3.3 V vs. SCE in CH_3CN). UV excitation of NMQ^+ sensitizer (λ_{max} = 315 nm for perchlorate salt) results in a strongly fluorescent excited state with a lifetime of ca. 13 ns and reduction potential of 2.7 V vs. SCE.[32] This excited state can be reductively quenched in the presence of large concentrations of co-donor, such as toluene, resulting in the initial formation of a the $NMQ^{\bullet}/Tol^{\bullet+}$ geminate radical pair, which efficiently separates in medium polarity solvents, such as dichloromethane, providing the free radical cation of toluene, a strong oxidizing reagent (2.35 V vs. SCE).[23] The reduced form of the photosensitizer, $NMQ^{\bullet}$ absorbs at ca. 540 nm and can be readily scavenged by dissolved O_2, resulting in the formation of NMQ^+ and $O_2^{\bullet-}$.[23, 27] Aromatic radical cations, including substituted benzenes are prone to dimerization, as shown in eq. 16 using toluene (Tol) as an

example. The dimer formation typically manifests in the growth of a characteristic absorption band in the NIR region, which is spectroscopically well separated from the absorption of the monomer radical cation.

$$Tol^{+} + Tol \rightleftarrows [Tol^{+}\cdots Tol] \quad (K_D) \qquad (16)$$

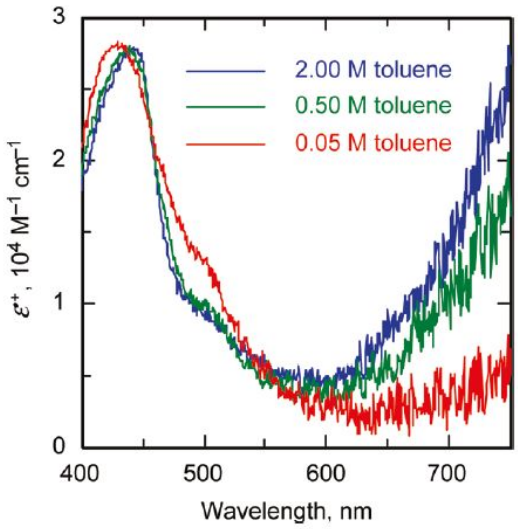

Figure 5. Transient absorption spectra of toluene radical cation (at 450 nm) and the $(toluene)_2^{\bullet+}$ dimer radical cation (in the NIR) in CH_3CN solutions containing various concentrations of toluene. Reprinted with permission from ref.[27] Copyright 2009 American Chemical Society.

The dimerization reaction has been observed for several substituted benzene radicals, however the value of K_D in acetonitrile was found to be relatively small, with the largest being 12 M^{-1} for benzene down to 2 M^{-1} for xylene cations, and negligibly small for biphenyls.[27] We will show later that the dimer formation can have a significant impact on the potential of the observed couple. However, this effect appears not to be significant for benzenes or biphenyls.

The photooxidation-driven redox equilibrium approach has been successfully used to obtain reduction potentials of several classes of organic compounds, including benzene and biphenyl derivatives,[23, 27-29] aromatic amines,[29] acetanilides and oxindoles[29]. The redox equilibrium method was shown to be a very accurate technique for measuring reduction potentials, with experimental errors as small as a few millivolts. For example, the cation potentials for a series of aromatic amines measured electrochemically, albeit reported by different research groups, appeared to be less accurate as compared to the equilibrium method (Figure 6). While a linear correlation between both sets can be clearly observed, the slope of the linear dependence is significantly greater than unity, indicating a systematic overestimation of potential values by

electrochemical measurements. The non-zero intercept of the plot could be indicative of differences in the reference potentials, either due to reference conversion or other factors.

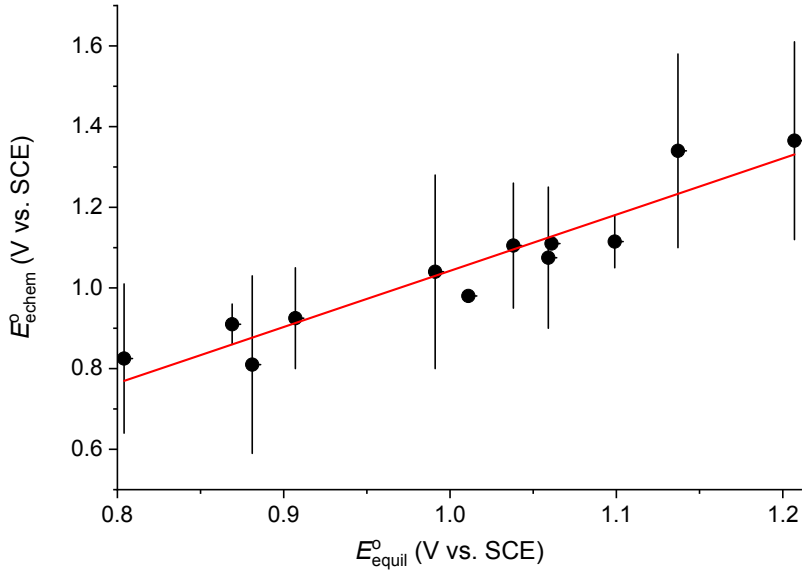

Figure 6. Reduction potentials of radical cations of aromatic amines measured electrochemically (E^o_{echem}) as reported in the literature plotted against the potentials measured by the redox equilibrium method (E^o_{equil}) .[29] Vertical lines represent the error bars for electrochemical potentials based on multiple reported values. The red line is a linear fit with a slope of 1.4 and $R^2 = 0.9$.

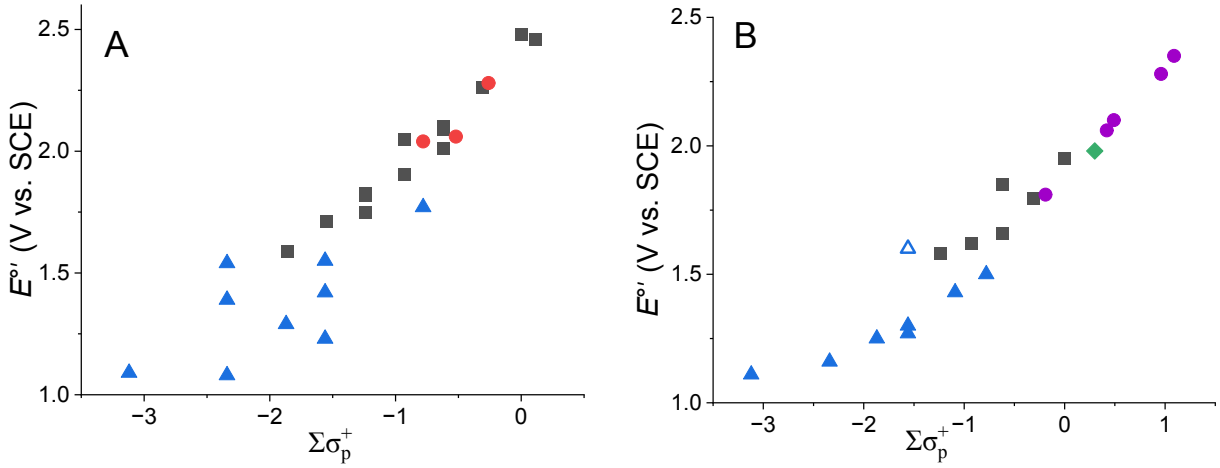

Figure 7. The correlation of formal reduction potentials ($E^{o\prime}$) of radical cations for: A. Benzene derivatives measured by redox equilibrium[29] and the Hammett parameter $\Sigma\sigma_p^+$.[33] The black squares are methyl-substituted benzenes; red circles represent *tert*-butyl substituted benzenes and blue triangles are methoxy-substituted benzenes; B. biphenyl derivatives measured by redox equilibrium[29] and the Hammett parameter, $\Sigma\sigma_p^+$.[33] The black squares are methyl-substituted biphenyls; purple circles represent ester substituted biphenyls, green diamond is 4,4'-dibromobiphenyl and blue triangles are methoxy-substituted biphenyls with substitutions in the meta- or para-positions. The open blue triangle is 2,2′-dimethoxybiphenyl.

The two particularly large datasets containing reduction potentials of substituted benzenes and biphenyls obtained by photochemical redox equilibrium can be used to explore correlation between potentials and physical parameters pertinent to substituent properties. For instance, good correlations between reduction potentials and Hammett parameters have been observed for a wide range of redox couples, especially within a homologous series of structurally related compounds, e.g., *para*-substituted ferrocene derivatives.[34] Figure 7A shows a correlation between reduction potentials of radical cations of substituted benzenes and the Hammett parameter, $\Sigma\sigma_p^+$ (which is a sum of individual σ_p^+ parameters for all substituents). A comprehensive compilation of Hammett parameters can be found in the review by Hansch, Leo and Taft.[33] While the applicability of Hammett parameters to compounds with different numbers of substituents and substitution positions may appear to be inappropriate, a reasonable linear correlation can still be observed for a series of substituted benzenes. A much tighter linear fit for methyl and *tert*-butyl substituents contrasts with the higher deviation from the fit for methoxy-substituted benzenes. Such differences could be attributed to the higher sensitivity of reduction potentials of benzenes containing methoxy groups to factors beyond electronic effects of substituents. It was noted, for example, that potentials of methoxy- and hydroxy- substituted ferrocenes[34] do not follow the general trend of $E^{o\prime} - \sigma_p^+$ and it was suggested that hydrogen bonding influences the redox properties of these cations. A similar behavior can be also observed for substituted biphenyls (Figure 7B), where a series of methoxy substituted biphenyls form a subset with a distinctly different $E^{o\prime} - \Sigma\sigma_p^+$ dependence from other functional groups. Another interesting "anomaly" evident from $E^{o\prime} - \Sigma\sigma_p^+$ dependence for biphenyl series is a substantially more positive potential for 2,2'-dimethoxybiphenyl radical cation as compared to other dimethoxybiphenyls with substituents in other positions. This effect is inherent to biphenyls and arises from forcing two phenyl rings out of planarity by the introduction of substituents into the ortho position. We will discuss this phenomenon in more detail in the next section.

Finally, it is interesting to compare reduction potentials of benzene and biphenyl radical cations. Dinnocenzo, Farid and Guirado[29] noted that potentials of benzenes and biphenyls bearing the same

substituents demonstrate excellent linear correlation with a slope of ca. 0.5 (Figure 8). They concluded that the reduction potentials of biphenyl radical cations are less sensitive to substitution as compared to benzenes. This was explained by the larger extent of radical delocalization in biphenyls across both phenyl groups.

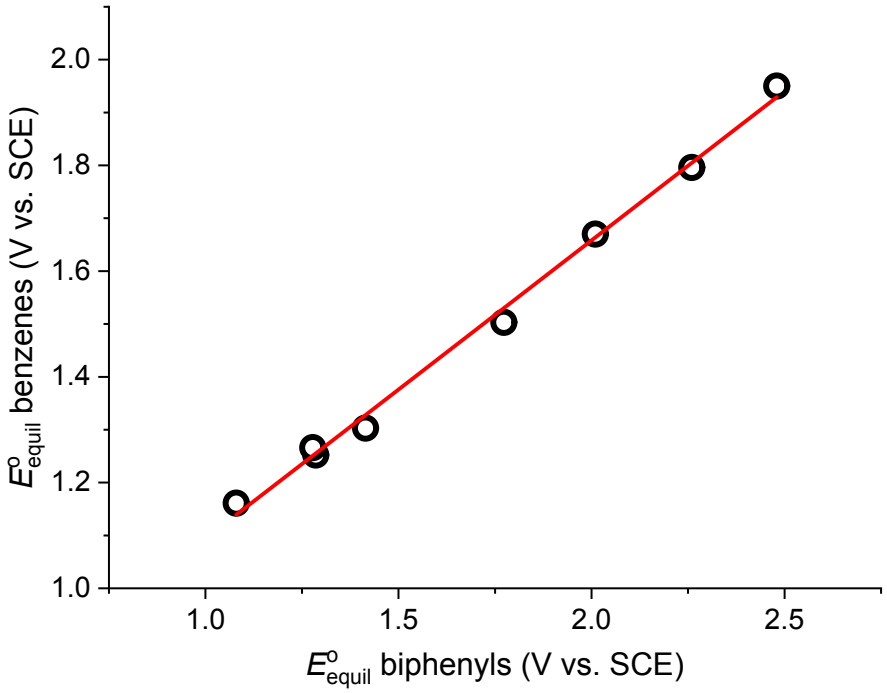

Figure 8. Reduction potentials of similarly substituted biphenyl (X axis) and benzene (Y axis) radical cations measured by photo redox equilibrium in CH_3CN. The red line represents a linear fit with a slope of 0.56 ± 0.2. Plotted from data in ref. [29].

Reduction potentials of oxidizing radicals determined by pulse radiolysis (PR) in organic media. Pulse radiolysis offers an alternative approach for measuring the potentials of reactive redox species present in solution. In contrast to photochemical methods, where photon energy is deposited directly into dissolved photooxidant precursor molecules, making them strong electron acceptors in their excited state, pulse radiolysis utilizes pulses of high energy electrons (typically in the MeV range) to induce ionization of predominantly solvent molecules when the concentration of solute is below ca. 1 M. The choice of solvent or selective radical scavengers can direct the solvent radiolysis towards exclusively oxidizing or reducing conditions, with solvent radical cations and solvated electrons being the ultimate redox reagents.[35, 36] The charge from solvent radicals can be rapidly scavenged by dissolved solute, resulting in desired oxidation states. This approach can be preferred to photochemical methods when photosensitizer absorption overlaps

with the absorption of solutes of interest or when access to potentials more positive than those available from sensitizers is needed.

It can be useful to briefly describe the mechanism of solvent ionization induced by high energy electrons. As electrons are emitted from an accelerator and are traveling through a liquid sample, their energy is partially transferred to solvent molecules, resulting in three primary energetic species: the solvent radical cation, a pre-solvated electron and an excited state of the solvent molecule (eqs. 17 – 18). Both reactions take place on an extremely short time scale, e.g., for water within 10^{-16} s.[36, 37] These initial events are followed by other reactions, and depending on the particular solvent, may include the formation of a solvation shell around an electron resulting in so-called solvated electron species, or an electron attachment to a solvent forming a solvent radical anion. The solvent excited states can fragment and form secondary radical species, e.g., OH• and H• radicals in the case of water, and the solvent radical cation can also fragment in a reaction with another solvent molecule, e.g., to OH• and H_3O^+ in water (see later).

$$\text{Solvent} \curvearrowright \text{Solvent}^{\bullet+} + e^-_{\text{pre-solvated}} \qquad (17)$$

$$\text{Solvent} \curvearrowright \text{Solvent}^* \qquad (18)$$

When pulse radiolysis is used for the production of oxidative radicals, the reduction potential of the solvent radical cation can be thought of as the most anodic "bias" generated in any given solvent. The reduction potentials of solvent cations cannot be easily determined and are known experimentally for only a few solvents, including xylene, toluene and benzene. On the other hand, the reduction potentials of radical cations of different classes of organic compounds can be measured experimentally and have been shown to correlate well with their gas phase ionization potentials.[22] We have compiled such a dependence for the most anodic couples known in Figure 9 and extrapolated the linear fit of experimental data to the more positive potentials with the purpose of predicting the reduction potentials of solvent radical cations. Interestingly, the predicted value for the potential of acetonitrile radical cation of ca. 4.15 V vs $Fc^{+/0}$ is very close to the potential of 4.22 V estimated from pulse radiolysis measurements,[38] and the value of 4.42 V from electrochemical measurements of solvent breakdown.[39] However, despite a good match for the acetonitrile radical, the potentials predicted from linear extrapolation in Figure 9 should be considered as a rough estimate, since such correlations are usually accurate only within a homologous series of organic compounds and may not include additional factors affecting the energetics of electron transfer.

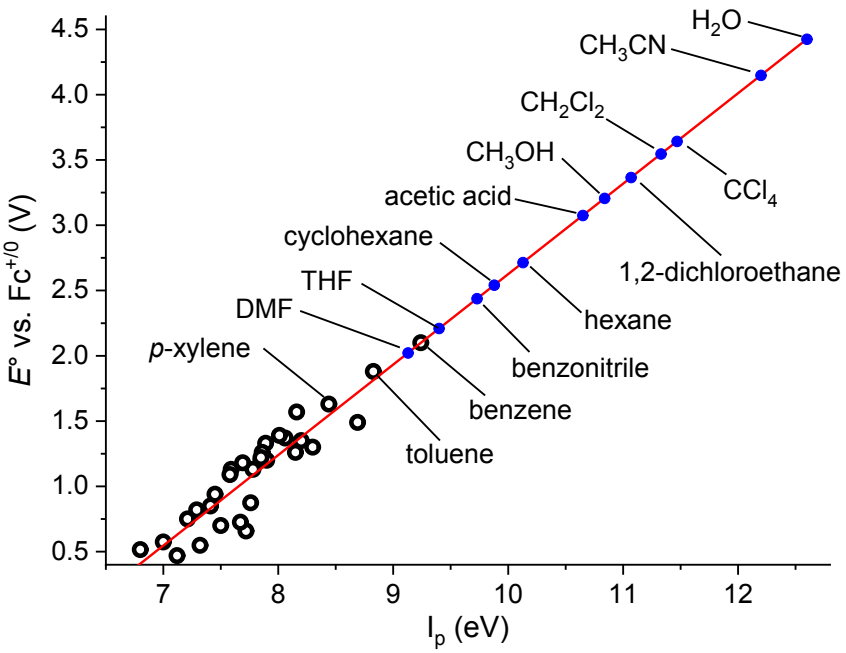

Figure 9. Correlation between gas-phase ionization potentials[40] and reduction potentials of radical cations. Black circles represent experimentally measured potentials and include the dataset reported in Figure 2 in addition to the selected redox pairs reported in the literature.[24, 27, 29] The linear fit through experimental data is shown as a red line with the following parameters: $E^{o} = -4.3 + 0.69 \times I_P$. Blue circles represent predicted values of reduction potentials of corresponding radical cations based on extrapolation of the linear fit.

Finally, while the reduction potentials of some solvent radicals are very positive, these radicals can never be utilized for driving oxidation of solute molecules due to their intrinsic instability. For example, water cation, $H_2O^{\bullet+}$ rapidly deprotonates on the time scale of ca. 200 fs,[41] resulting in OH• and H_3O^+, with the former being the primary oxidant during radiolysis of water. A similar reactivity is proposed for $CH_3CN^{\bullet+}$ radical, which is extremely acidic (p*K*a of ca. – 45) and rapidly loses a proton to form the $^{\bullet}CH_2CN$ radical.[38] The fragmentation of an excited acetonitrile molecule also produces CH_3•, CN• and H•, resulting in a complex mixture of radicals with a wide range of reactivities. The radical cations of halogenated solvents including chloroform, dichloroethane, dichloromethane, and carbon tetrachloride are relatively stable and are typically used in radiolytic oxidation of various substrates.[35, 42, 43] Low polarity solvents, including alkanes produce very low yields of cations and anions due to their rapid recombination within the solvent cage, resulting in mostly solvent excited states and neutral radical fragments.[44, 45]

We have utilized PR for understanding the redox properties of organic radical cations in halogenated solvents, e.g., dichloroethane.[24] First, the accuracy of our approach was verified by comparing reduction

potentials of five radical cations measured by redox equilibrium to $E_{1/2}$ values obtained from reversible CVs. Figure 10 demonstrates excellent match between potentials measured by both techniques, confirming the applicability of the pulse radiolysis equilibrium approach for determination of reduction potentials of different classes of organic radicals. Furthermore, this dataset demonstrates that the 5−compound redox ladder spanning across 300 mV of potential window introduces an uncertainty of less than 5 mV for the most positive couple.

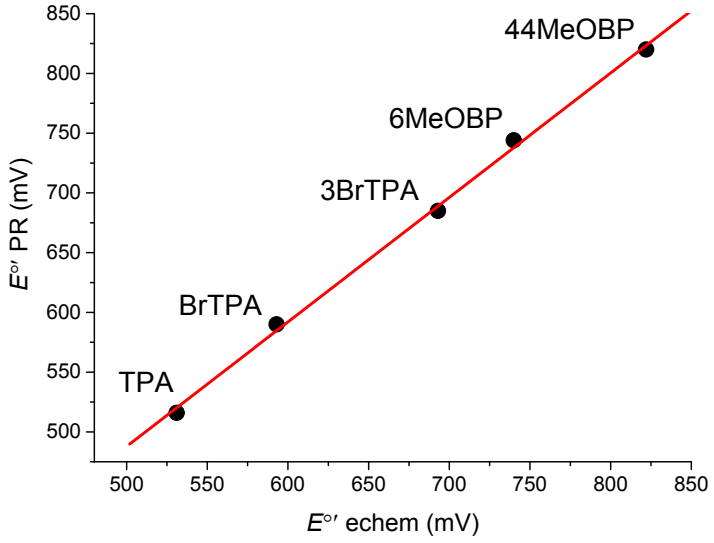

Figure 10. Formal reduction potentials $E^{o\prime}$ (vs. $Fc^{+/0}$) of radical cations determined by PR equilibria measurements as compared to potentials determined from reversible CV waves ($E^{o\prime} = E_{1/2}$). All measurements are performed in air-free DCE with 0.1 M $TBAPF_6$ and 0.1M 1,4-pentadiene. The red line represents a linear fit of the data (slope 1.04 ± 0.03, intercept -33 ± 20, and R^2 = 0.998). Reprinted with permission from ref [24]. Copyright 2023 American Chemical Society.

Our group has utilized the PR method to measure the potentials of two homologous series of substituted biphenyl derivatives. In particular, the $E^{o\prime} - \Sigma\sigma_p^+$ correlation was explored by systematically varying the substituents in the same position in order to separate electronic and steric effects on redox properties. Interestingly, the $E^{o\prime} - \Sigma\sigma_p^+$ plot for *para*-substituted biphenyls is not linear and exhibits saturation at more positive potentials (Figure 11A). The introduction of substituents into the 2,2′ positions shifts the potentials of cations ca. 200 mV more positive, maintaining the same saturation trend as the $\Sigma\sigma_p^+$ values increase.

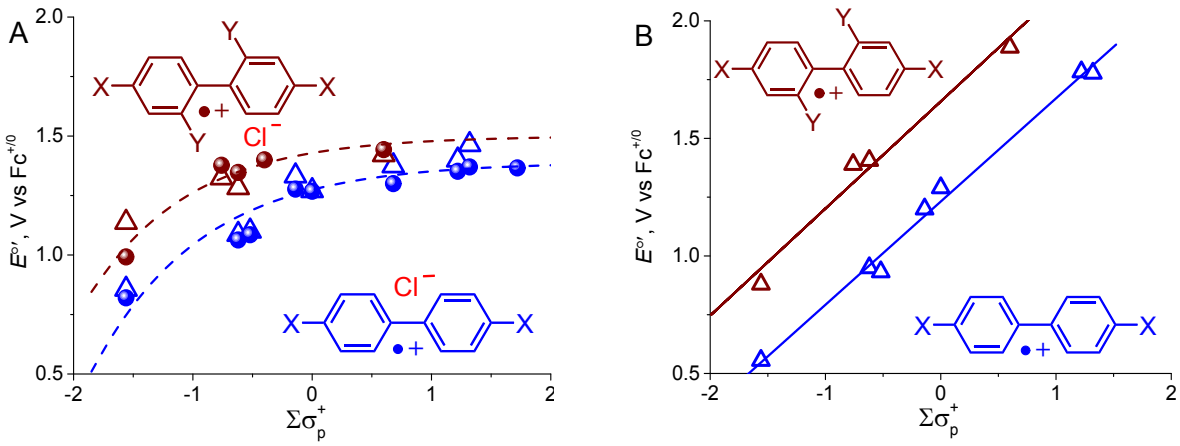

Figure 11. A) Reduction potentials of 4,4′–X_2 (blue spheres) and 2,2′–Y_2–4,4′–X_2 (wine spheres) biphenyl cations determined by PR as compared to potentials predicted by theory for corresponding [$BP^{\bullet+}$… Cl^-] pairs (triangles) plotted as a function of $\sum\sigma_p^+$. Computed potentials are adjusted relative to experimental values of **BP** for the 4,4′–X_2 series and **22MeBP** for the 2,2′–Y_2–4,4′–X_2 dataset. Dotted lines are for visual guidance only. B) Reduction potentials of 4,4′–X_2 (blue triangles) and 2,2′–Y_2–4,4′–X_2 biphenyls (wine triangles) predicted by theoretical calculations in the absence of Cl^-. Solid lines represent linear fits. Reprinted with permission from ref [24]. Copyright 2023 American Chemical Society.

The nonlinearity of the $E^{o\prime} - \Sigma\sigma_p^+$ plot was found to be surprising, since the analysis of previously reported potentials for a variety of organic radical cations demonstrated reasonable linear correlations with $\Sigma\sigma_p^+$ (Fig. 7), and the DFT-predicted potentials[24] (at M06-2X/def2-TZVPP level of theory)[46, 47] of the same radicals were found to vary linearly with the Hammett parameter (Figure 11B). This saturation trend has been explained by the existence of a strong interaction between radiolytically produced chloride anion (Cl^-) and the organic radical cation, leading to the stabilization of the positive charge. It was argued that the electrostatic interaction between two ions was not sufficiently strong to explain the significant stabilization of 100 mV – 400 mV, and that an additional interaction in the form of hemicolligation is necessary to explain the observed changes in potentials. The hemicolligation of radicals with other species, $X^{\bullet} + X^- \rightleftarrows [X]_2^{\bullet-}$ has been well studied for inorganic radicals, and association constants for this equilibrium in water can be substantial, especially when halide radicals are involved, e.g., $K_{HC}(Cl) = 1.4\times10^5$ M^{-1}; $K_{HC}(I) = 1.3\times10^5$ M^{-1}; and $K_{HC}(Br) = 3.9\times10^5$ M^{-1}.[48, 49] In organic solvents, these values can be orders of magnitude higher compared to aqueous solvents.[50] It was proposed that the combined effect of hemicolligation and ion pairing can be rationalized by the overall stabilization free energy, ΔG_{stab} which includes contributions of ion pairing and hemicolligation: $\Delta G_{stab} = \Delta G_{IP} + \Delta G_{HC}$, and the resulting effect on potential can be described by eq. 19.

$$E = E^{o} - 0.059 \log (1 + K_{HC}K_{IP}[Cl^{-}]) \quad (19)$$

In addition to electronic effects of substituents and influence of ion-paired halide anion, the reduction potentials of biphenyl radical cations were found to depend on the conjugation between the two phenyl rings. When substituents are introduced to, for example, the 2,2′ positions, forcing two benzene rings out of planarity, the potential of cations increases by about 200 mV (Figure 11A). This effect can be rationalized based on the known behavior of biphenyls to adapt a more planar geometry upon oxidation due to delocalization of positive charge across both aromatic systems, which brings down the reduction potential of the cation.[51-53] When two aromatic systems are forced out of conjugation, the reduction potential rises, approaching in an extreme case the potential of the corresponding substituted benzene molecule.

Application of highly oxidizing radicals in mechanistic studies of water oxidation catalysis. Catalytic water oxidation has become a prominent field in the area of renewable energy research, leading to remarkable advances in the development of efficient molecular and heterogeneous catalysts.[1, 54] These advances would not be possible without in-depth understanding of catalytic mechanism and properties of key redox intermediates involved in water oxidation. The generation of such intermediates often requires access to powerful oxidation reagents, and while some redox reagents, including strong oxidants can be prepared and isolated in their metastable forms,[55, 56] most strong oxidants exist on a transient time scale (<< 1 s) and their production requires high energy inputs, i.e., in the form of photoexcitation or ionizing radiation. Radiolysis of water provides a convenient and controllable way for the generation of highly energetic solvent-derived radicals, which can be converted into a wide variety of secondary oxidants (Table 1).[3, 36] Eqs. 20-22 show the conversion of hydrated electrons into oxidizing $OH^{\bullet}$ radicals, and their use in oxidizing a substrate.

$$H_2O \text{ √√⟶ } e_{aq}^{-}, OH^{\bullet}, H^{\bullet}, H_2, H_2O_2 \quad (20)$$

$$e_{aq}^{-} + N_2O \rightarrow N_2 + H_2O + O^{\bullet -} \rightarrow OH^{\bullet} + OH^{-} \quad (21)$$

$$OH^{\bullet} + \text{substrate} = \text{substrate}^{\bullet +} + OH^{-} \quad (22)$$

The primary oxidant produced by water radiolysis is the hydroxyl radical $OH^{\bullet}$, with a standard reduction potential of ca. 1.9 V vs. NHE for the $OH^{\bullet}/OH^{-}$ couple. It is important to note that the formal potential of hydroxyl radical shows Nernstian dependence on proton concentration, reaching 2.72 V at p*H* 0. Despite being a strong oxidant, $OH^{\bullet}$ tends to engage in reactions other than simple electron transfer, notably addition to unsaturated bonds or H-atom abstraction.[57, 58] This reactivity may be detrimental in cases where a simple one-electron oxidation of a catalyst molecule is desired, which is often the case during investigation of water oxidation mechanisms. An example of such reactivity has been observed during a series of studies of

the dimeric μ-oxo-bridged ruthenium complex, *cis,cis*-$[(bpy)_2(H_2O)Ru\text{-}O\text{-}Ru(OH_2)(bpy)_2]^{4+}$ (also known as the Ru "blue dimer") at Brookhaven's pulse radiolysis facility.[3] Figure 12 shows a sequence of reactions initiated by the addition of OH• to one of the pyridine rings of the Ru blue dimer. This step is followed by electron transfer from the aromatic radical to the metal center, and proton loss resulting in hydroxy-substituted pyridine and a reduced metal center, which constitutes an overall "oxidant-induced reduction" reaction.

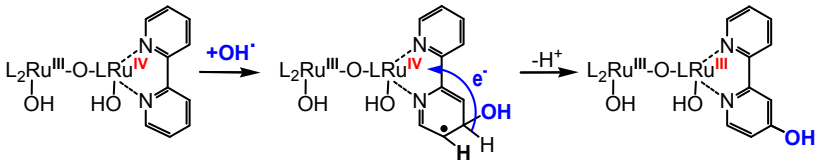

Figure 12. Reduction of the Ru blue dimer by OH•.[3]

Since the primary utility of pulse radiolysis is to provide access to catalytic intermediates in various oxidation states, oxidants which mainly engage in electron transfer reactions are desired. Fortunately, a wide variety of secondary strong oxidants can be produced from reaction of OH• with aqueous solutions of inorganic salts (eq. 22 and Table 1).

Table 1. Potentials and selected hemicolligation equilibrium constants of strongly oxidizing radicals in aqueous solution.

Couple	$E°$, V NHE	Hemicolligation (HC) Equilibria	K_{HC}[48]
$H_2PO_4^{\bullet}/H_2PO_4^-$	2.75[48]		
$OH^{\bullet}, H^+/H_2O$	2.72[48]		
$NO_3^{\bullet}/NO_3^-$	2.47[48]		
$SO_4^{\bullet-}/SO_4^{2-}$	2.44[48, 59]		
$Cl^{\bullet}/Cl^-$	2.43[48]	$Cl^{\bullet} + Cl^- \rightleftarrows Cl_2^{\bullet-}$	1.4×10^5
$ClO_3^{\bullet}/ClO_3^-$	2.38[48]		
$Tl^{\bullet 2+}/Tl^+$	2.22[48, 60]		
$Br^{\bullet}/Br^-$	1.96[48]	$Br^{\bullet} + Br^- \rightleftarrows Br_2^{\bullet-}$	3.9×10^5
$OH^{\bullet}/OH^-$	1.89[48, 61]	$OH^{\bullet} + Cl^- \rightleftarrows ClOH^{\bullet-}$ $OH^{\bullet} + Br^- \rightleftarrows BrOH^{\bullet-}$ $OH^{\bullet} + Tl^+ \rightleftarrows TlOH^{\bullet+}$	0.7 320 5.8×10^3
$TeO_3^{\bullet-}/ TeO_3^{2-}$	1.74[48]		
$SeO_3^{\bullet-}/ SeO_3^{2-}$	1.68[48, 62]		
$Br_2^{\bullet-}/2Br^-$	1.63[48]		
$SCN^{\bullet}/SCN^-$	1.61[48]	$SCN^{\bullet} + SCN^- \rightleftarrows (SCN)_2^{\bullet-}$	2×10^5
$CO_3^{\bullet-}/ CO_3^{2-}$	1.55[59]		
$ClO^{\bullet}/ClO^-$	1.39[48]		
$I^{\bullet}/I^-$	1.35[48]	$I^{\bullet} + I^- \rightleftarrows I_2^{\bullet-}$	1.4×10^5

Halide radicals ($X^{\bullet}$) are excellent one-electron oxidants and rarely exhibit any other reactivity in aqueous solutions, contrary to more diverse reactivity in organic solvents.[63] However, halide radicals readily hemicolligate with anions X^{-}, which are used as precursors for radical generation, forming $X_2^{\bullet-}$ species. Depending on the hemicolligation constant and concentration of halide anion, $X_2^{\bullet-}$ can be the primary oxidant under given conditions, with the formal reduction potential adjusted to the value of K_{HC} (eq. 23):

$$E^{o\prime} = E^{o} - 0.059 \log (K_{HC}) \quad (23)$$

One of the most powerful oxidants which can be produced by pulse radiolysis in water is the sulfate radical, $SO_4^{\bullet-}$. Interestingly, it is formed by the reduction of persulfate dianion $[S_2O_8]^{2-}$ with a hydrated electron (eq. 24):

$$[S_2O_8]^{2-} + e_{aq}^{-} \rightarrow SO_4^{\bullet-} + SO_4^{2-} \quad (24)$$

Alternitevly, $SO_4^{\bullet-}$ can be generated photochemically, for example, by electron transfer from a photoexcited chromophre such as $*[Ru(bpy)_3]^{2+}$. However, it is typically rapidly consumed by chromophore molecules in their ground state to form $[Ru(bpy)_3]^{3+}$, which acts as a secondary oxidant towards water oxidation catalysts.[64, 65] Thermal oxidations of substrates by persulfate are typically very slow despite favorable thermodynamic driving forces, which can be explained by very large values of inner-sphere reorganization energy for electron transfer.[64]

The carbonate radical ($CO_3^{\bullet-}$) is another useful oxidant which can be cleanly produced by reaction of $OH^{\bullet}$ with bicarbonate in the pH range 9 – 12, and exhibits clean electron transfer reactivity without engaging in side-reactions, such as hemicolligaiton. We have successfully utilized the reactivity of $CO_3^{\bullet-}$ to study intermediates of water oxidation catalysts in high oxidation states.[66-68] For example, Figure 13 shows the UV-Vis spectra of $[Ru^{II}(H_2O)(NPM)(4\text{-pic})_2]^{2+}$ water oxidation catalyst and its one- and two-electron oxidized forms produced by pulse radiolysis in aqeous bicarbonate buffer at pH 10. The fast generation of the oxidized form of the catalyst allowed identification of unstable $[Ru^{III}(OH)(NPM)(4\text{-pic})_2]^{2+}$ intermediate which was found to disproportinate to form $[Ru^{IV}(O)(NPM)(4\text{-pic})_2]^{2+}$. In addition, the $Ru^{IV}(O)$ intermediate was found to be reactive towards OH^{-}, a reactivity which could not be directly probed by other techniques.[66]

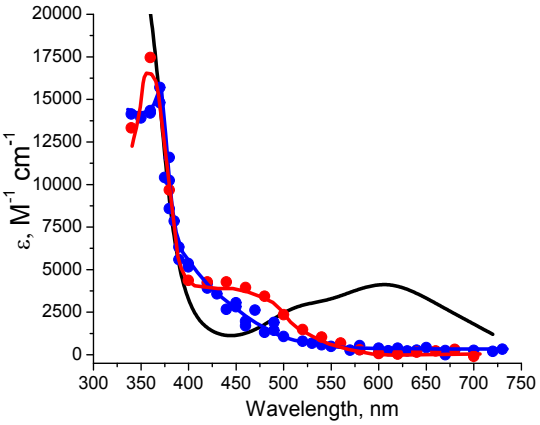

Figure 13. UV-vis spectra of $[Ru(H_2O)(NPM)(4\text{-pic})_2]^{2+}$ water oxidation catalyst (black) and its one-electron oxidized species (red) and two-electron oxidized species (blue) generated by pulse radiolysis in aqueous bicarbonate buffer at pH 10. Reprinted with permission from ref.[66] Copyright 2011 American Chemical Society.

In summary, this overview highlights the properties and reactivity of reactive oxidizing radicals in aqueous and organic solutions. The limitations of voltammetry methods for determining accurate values of reduction potentials for couples involving reactive radical intermediates are presented through a kinetic analysis of cyclic voltammogram shapes using the kinetic zone diagram, introduced by Savéant. The kinetic coupling of a chemical step to an electron transfer reaction at an electrode creates challenges in obtaining accurate values of standard reduction potentials even if the shape of the *I*–*V* (electrochemical current vs. potential) curve appears to be reversible. While AC voltammetry can provide an alternative electrochemical approach for measurements of highly reactive redox couples, redox equilibrium methods based on transient generation of strong oxidants in solution are more versatile in decoupling fast electrochemical and chemical elementary steps, and can yield accurate values of reduction potentials for reactive couples. The transient redox equilibrium experiment can be initiated photochemically through generation of strong photooxidant or by pulse radiolysis, through ionization of solvent molecules, followed by charge transfer to a solute. While radical cations with potentials as positive as ca. 4 V vs. $Fc^{+/0}$ can be initially produced using these techniques, many of them experience extremely fast decomposition, e.g., deprotonation, resulting in less oxidizing species. Aromatic radical cations are among the strongest organic oxidants, with reduction potentials surpassing 2 V vs. $Fc^{+/0}$. The potentials of these radicals correlate well with Hammett $\Sigma\sigma_p^+$ parameter as well as gas phase ionization potentials. Both correlations can be used to estimate the redox properties of unknown couples within a homologous series of compounds. Organic radical cations are found to experience strong hemicolligation with halide anions, such as Cl^-, which can substantially attenuate their

reduction potentials. This is a common phenomenon between organic and inorganic oxidative radicals, but it was found to be more pronounced in the case of organic cations. Finally, the time resolution capabilities of transient methods not only allow the fast production of reactive radicals but also provide a powerful approach for studying their reactivity with different substrates. For example, the generation of transient intermediates of water oxidation catalysts has been achieved by means of the radiolytic production of oxidizing radicals in aqueous solutions.

Acknowledgements.

We thank Dr. David Grills for insightful discussions and his valuable comments during the preparation of this manuscript. This work, and use of the LEAF facility of the BNL Accelerator Center for Energy Research, was carried out at Brookhaven National Laboratory and supported by the U.S. Department of Energy (DOE), Office of Science, Office of Basic Energy Sciences, Division of Chemical Sciences, Geosciences, & Biosciences, under contract DE-SC0012704.

Data availability

The data supporting this article and used to generate Figures 2, 6-9 have been included as part of the Supplementary Information.

References

1. R. Matheu, P. Garrido-Barros, M. Gil-Sepulcre, M. Z. Ertem, X. Sala, C. Gimbert-Suriñach and A. Llobet, *Nat. Rev. Chem.*, 2019, **3**, 331-341.
2. K. Yamaguchi, M. Shoji, H. Isobe, T. Kawakami, K. Miyagawa, M. Suga, F. Akita and J.-R. Shen, *Coord. Chem. Rev.*, 2022, **471**, 214742.
3. D. E. Polyansky, J. K. Hurst and S. V. Lymar, *Eur. J. Inorg. Chem.*, 2014, DOI: 10.1002/ejic.201300753, 619-634.
4. S. Ahn, A. Yun, D. Ko, V. Singh, J. M. Joo and H. R. Byon, *Chem. Soc. Rev.*, 2024, DOI: 10.1039/d4cs00585f.
5. B. Liu, Y. J. Li, G. C. Jia and T. S. Zhao, *Electrochem. Energy Rev.*, 2024, **7**.
6. A. G. Chmielewski and M. M. Szołucha, *Radiat. Phys. Chem.*, 2016, **124**, 235-240.
7. M. K. Wilsey, T. Taseska, Z. Meng, W. Yu and A. M. Müller, *Chem. Commun.*, 2023, **59**, 11895-11922.
8. N. A. Romero and D. A. Nicewicz, *Chem. Rev.*, 2016, **116**, 10075-10166.
9. C. K. Prier, D. A. Rankic and D. W. C. MacMillan, *Chem. Rev.*, 2013, **113**, 5322-5363.
10. L. Zhang, Y. Qiu, W.-G. Liu, H. Chen, D. Shen, B. Song, K. Cai, H. Wu, Y. Jiao, Y. Feng, J. S. W. Seale, C. Pezzato, J. Tian, Y. Tan, X.-Y. Chen, Q.-H. Guo, C. L. Stern, D. Philp, R. D. Astumian, W. A. Goddard and J. F. Stoddart, *Nature*, 2023, **613**, 280-286.
11. D. C. Grills, D. E. Polyansky and E. Fujita, *ChemSusChem*, 2017, **10**, 4359-4373.
12. R. A. Marcus and N. Sutin, *Biochim. Biophys. Acta, Rev. Bioenerg.*, 1985, **811**, 265-322.
13. A. J. Bard and L. R. Faulkner, *Electrochemical Methods. Fundamentals and Applications*, John Wiley & Sons, Inc, New York, 2001.
14. J.-M. Savéant, *Elements of Molecular and Biomolecular Electrochemistry: An Electrochemical Approach to Electron Transfer Chemistry*, John Wiley & Sons, 2006.
15. P. Zanello, *Inorganic Electrochemistry: Theory, Practice and Application*, Royal Society of Chemistry, Cambridge, 2003.
16. F. Marken, A. Neudeck and A. M. Bond, in *Electroanalytical Methods*, ed. F. Scholz, Springer, Heidelberg, 2010, pp. 57-106.
17. Á. Molina and J. González, *Pulse Voltammetry in Physical Electrochemistry and Electroanalysis*, Springer Cham, Heidelberg, 2016.
18. A. M. Bond, R. J. O'Halloran, I. Ruzic and D. E. Smith, *Anal. Chem.*, 1976, **48**, 872-883.
19. A. M. Bond and D. E. Smith, *Anal. Chem.*, 1974, **46**, 1946-1951.
20. E. Ahlberg and V. D. Parker, *Acta Chem. Scand. Ser. B*, 1980, **34**, 97-102.
21. E. Ahlberg and V. D. Parker, *Acta Chem. Scand. Ser. B*, 1980, **34**, 91-96.
22. S. Fukuzumi, K. Ohkubo, H. Imahori and D. M. Guldi, *Chem. Eur. J.*, 2003, **9**, 1585-1593.
23. G. Guirado, C. N. Fleming, T. G. Lingenfelter, M. L. Williams, H. Zuilhof and J. P. Dinnocenzo, *J. Am. Chem. Soc.*, 2004, **126**, 14086-14094.
24. D. E. Polyansky, G. F. Manbeck and M. Z. Ertem, *J. Phys. Chem. A*, 2023, **127**, 7918-7927.
25. J. H. Espenson, *Chemical kinetics and reaction mechanisms*, McGraw-Hill, 1981.
26. I. R. Gould, Z. M. Wosinska and S. Farid, *Photochem. Photobiol.*, 2006, **82**, 104-109.
27. P. B. Merkel, P. Luo, J. P. Dinnocenzo and S. Farid, *J. Org. Chem.*, 2009, **74**, 5163-5173.
28. P. Luo, J. P. Dinnocenzo, P. B. Merkel, R. H. Young and S. Farid, *J. Org. Chem.*, 2012, **77**, 1632-1639.
29. P. Luo, E. C. Feinberg, G. Guirado, S. Farid and J. P. Dinnocenzo, *J. Org. Chem.*, 2014, **79**, 9297-9304.
30. D. Kim, V. Q. Dang and T. S. Teets, *Chem. Sci.*, 2024, **15**, 77-94.
31. I. R. Gould, D. Ege, J. E. Moser and S. Farid, *J. Am. Chem. Soc.*, 1990, **112**, 4290-4301.
32. U. C. Yoon, S. L. Quillen, P. S. Mariano, R. Swanson, J. L. Stavinoha and E. Bay, *J. Am. Chem. Soc.*, 1983, **105**, 1204-1218.

33. C. Hansch, A. Leo and R. W. Taft, *Chem. Rev.*, 1991, **91**, 165-195.
34. M. Emília, N. P. R. A. Silva, A. J. L. Pombeiro, J. J. R. F. da Silva, R. Herrmann, N. Deus, T. J. Castilho and M. F. C. G. Silva, *J. Organomet. Chem.*, 1991, **421**, 75-90.
35. A. J. Swallow, in *Radiation Chmistry*, eds. M. A. J. Rodgers and Farhataziz, VCH, New York, 1987, pp. 351-375.
36. G. V. Buxton, in *Radiation Chemistry. Principles and Applications*, eds. Farhataziz and M. A. J. Rodgers, VCH, New York, 1987.
37. K. Bobrowski, in *Applications of Ionizing Radiation in Materials Processing*, eds. Y. Sun and A. G. Chmielewski, Institute of Nuclear Chemistry and Technology, Warszawa, 2017, vol. 1.
38. D. C. Grills and S. V. Lymar, *Phys. Chem. Chem. Phys.*, 2018, **20**, 10011-10017.
39. J. Cassidy, S. B. Khoo, S. Pons and M. Fleischmann, *J. Phys. Chem.*, 1985, **89**, 3933-3935.
40. P. J. Linstrom and W. G. Mallard, *NIST Chemistry WebBook, NIST Standard Reference Database Number 69*, National Institute of Standards and Technology, Gaithersburg, retrieved November 13, 2024.
41. J. L. Li, Z. G. Nie, Y. Y. Zheng, S. Dong and Z. H. Loh, *J. Phys. Chem. Lett.*, 2013, **4**, 3698-3703.
42. M. J. Bird, A. R. Cook, M. Zamadar, S. Asaoka and J. R. Miller, *Phys. Chem. Chem. Phys.*, 2020, **22**, 14660-14670.
43. T. Sumiyoshi, N. Sugita, K. Watanabe and M. Katayama, *Bull. Chem. Soc. Jpn.*, 1988, **61**, 3055-3059.
44. L. H. Gevantman and R. R. Williams, *J. Phys. Chem.*, 1952, **56**, 569-574.
45. B. C. Lemotais and C. D. Jonah, *Radiat. Phys. Chem.*, 1989, **33**, 505-517.
46. D. Rappoport and F. Furche, *J. Chem. Phys.*, 2010, **133**.
47. F. Weigend and R. Ahlrichs, *Phys. Chem. Chem. Phys.*, 2005, **7**, 3297-3305.
48. D. A. Armstrong, R. E. Huie, W. H. Koppenol, S. V. Lymar, G. Merényi, P. Neta, B. Ruscic, D. M. Stanbury, S. Steenken and P. Wardman, *Pure Appl. Chem.*, 2015, **87**, 1139-1150.
49. D. Stanbury, in *Physical inorganic chemistry. Reactions, processes, and applications*, ed. A. Bakac, Wiley, 2010.
50. A. Treinin and E. Hayon, *Int. J. Radiat. Phys. Chem.*, 1975, **7**, 387-393.
51. L. Zhang, G. H. Peslherbe and H. M. Muchall, *Can. J. Chem.*, 2010, **88**, 1175-1185.
52. C. W. Lee, D. Pan, L. C. T. Shoute and D. L. Phillips, *Res. Chem. Intermed.*, 2001, **27**, 485-501.
53. A. Nilsson, U. Palmquist and A. Ronlan, *J. Am. Chem. Soc.*, 1975, **97**, 3540-3541.
54. S. Ye, C. M. Ding, M. Y. Liu, A. Q. Wang, Q. G. Huang and C. Li, *Adv. Mater.*, 2019, **31**.
55. A. R. Parent, R. H. Crabtree and G. W. Brudvig, *Chem. Soc. Rev.*, 2013, **42**, 2247-2252.
56. N. G. Connelly and W. E. Geiger, *Chem. Rev.*, 1996, **96**, 877-910.
57. S. Gordon, K. H. Schmidt and E. J. Hart, *J. Phys. Chem.*, 1977, **81**, 104-109.
58. P. Neta and L. M. Dorfman, in *Radiation Chemistry*, American Chemical Society, 1968, vol. 81, ch. 15, pp. 222-230.
59. D. M. Stanbury, *Adv. Inorg. Chem.*, 1989, **33**, 69-138.
60. H. A. Schwarz, D. Comstock, J. K. Yandell and R. W. Dodson, *J. Phys. Chem.*, 1974, **78**, 488-493.
61. H. A. Schwarz and R. W. Dodson, *J. Phys. Chem.*, 1984, **88**, 3643-3647.
62. U. K. Klaning and K. Sehested, *J. Phys. Chem.*, 1986, **90**, 5460-5464.
63. P. S. Skell, H. N. Baxter, J. M. Tanko and V. Chebolu, *J. Am. Chem. Soc.*, 1986, **108**, 6300-6311.
64. A. Lewandowska-Andralojc and D. E. Polyansky, *J. Phys. Chem. A*, 2013, **117**, 10311-10319.

65. A. Lewandowska-Andralojc, D. E. Polyansky, R. F. Zong, R. P. Thummel and E. Fujita, *Phys. Chem. Chem. Phys.*, 2013, **15**, 14058-14068.
66. D. E. Polyansky, J. T. Muckerman, J. Rochford, R. Zong, R. P. Thummel and E. Fujita, *J. Am. Chem. Soc.*, 2011, **133**, 14649–14665.
67. M. K. Tsai, J. Rochford, D. E. Polyansky, T. Wada, K. Tanaka, E. Fujita and J. T. Muckerman, *Inorg. Chem.*, 2009, **48**, 4372-4383.
68. Y. M. Badiei, D. E. Polyansky, J. T. Muckerman, D. J. Szalda, R. Haberdar, R. F. Zong, R. P. Thummel and E. Fujita, *Inorg. Chem.*, 2013, **52**, 8845-8850.

Data availability

The data supporting this article and used to generate Figures 2, 6-9 have been included as part of the Supplementary Information.